Hetero-Bis-Conjugation of Bioactive Molecules to Half-Sandwich Ruthenium(II) and Iridium(III) Complexes Provides Synergic Effects in Cancer Cell Cytotoxicity

Lorenzo Biancalana,[a,] Hana Kostrhunova,[b] Lucinda K. Batchelor,[c] Mouna Hadiji,[c] Ilaria Degano,[a] Guido Pampaloni, [a] Stefano Zacchini,[d] Paul J. Dyson,[c] Viktor Brabec,[b,*] Fabio Marchetti [a]*

[a] *Dipartimento di Chimica e Chimica Industriale, Università di Pisa, Via G. Moruzzi 13, I-56124 Pisa, Italy.*

[b] *Czech Academy of Sciences, Institute of Biophysics, Kralovopolska 135, CZ-61265 Brno, Czech Republic.*

[c] *Institut des Sciences et Ingénierie Chimiques, Ecole Polytechnique Fédérale de Lausanne (EPFL), CH-1015 Lausanne, Switzerland.*

[b] *Dipartimento di Chimica Industriale "Toso Montanari", Università di Bologna, Viale Risorgimento 4, I-40136 Bologna, Italy.*

Corresponding Authors

*E-mail addresses: lorenzo.biancalana@unipi.it , brabec@ibp.cz

Abstract

Four bipyridine-type ligands variably derivatized with two bioactive groups (taken from ethacrynic acid, flurbiprofen, biotin and benzylpenicillin) were prepared via sequential esterification steps from commercial 2,2′-bipyridine-4,4′-dicarboxylic acid and subsequently coordinated to ruthenium(II) *p*-cymene and iridium(III) pentamethylcyclopentadienyl scaffolds. The resulting complexes were isolated as nitrate salts in high yields and fully characterized by analytical and spectroscopic methods. NMR and MS studies in aqueous solution and in cell culture medium highlighted a substantial stability of ligand coordination and a slow release of the bioactive fragments in the latter case. The complexes were assessed for their antiproliferative activity on four cancer cell lines, showing cytotoxicity to the low micromolar level (equipotent to cisplatin). Additional biological experiments revealed a multimodal mechanism of action of the investigated compounds, involving DNA metalation as well as enzyme inhibition by the organic fragments released following cellular uptake. Synergic effects provided by specific combinations of metal and bioactive fragments were identified, pointing towards an optimal ethacrynic acid/flurbiprofen combination for both Ru(II) and Ir(III) complexes.

Keywords: bioorganometallic chemistry, ruthenium(II) arene, iridium(III) cyclopentadienyl, bioactive ligand, cytotoxicity, anticancer metal compounds; enzyme inhibition.

Introduction

Conjugation of biologically-active metal scaffolds and organic molecules is a well-documented strategy to enhance the therapeutic effects of the resulting compound, and is widely applied to cytotoxic metal complexes investigated as potential anticancer agents.[1] In general, 'bioactive molecules' are both those possessing a pharmacological function on their own (providing a *multi-action* compound) and those behaving as 'vectors' for increasing the localization of a drug (providing a *targeted* compound). This approach to combine bioactive molecules with metal complexes met with success in several cases where considerable synergic effects have been observed for the bioconjugates with respect to non-functionalized metal complexes and/or co-administration of the two individual components.[2] The mechanism of action of such derivatives is likely multimodal and often largely unknown, with respect to the interplay of the metal center and the bioactive ligands.

In this regard, the incorporation of *multiple* bioactive molecules on a monometallic structure is expected to further improve anticancer activity, particularly if the former are endowed with different (complementary) modes of action and cellular targets.[3] In the last few years, several platinum(IV) compounds of this kind have been prepared, featuring various combinations of fragments targeting specific enzymes, receptors, cellular compartments as well as organic antineoplastic agents.[4] From a synthetic standpoint, these complexes are obtained by sequential derivatization of *trans* (axial) Pt−OH groups with ester or carbamate linkages from common Pt(IV) precursors (Scheme 1a). The anticancer activity of such multi-targeted/multi-action derivatives has been extensively investigated; some of these were able to outperform reference platinum drugs in terms of cancer cell cytotoxicity, also in 3D cell cultures, and activity against primary tumors *in vivo*.[4b-d,h]

Inspired by the same principle, we recently reported a series of platinum(II) complexes containing (hetero)bis-functionalized bipyridine ligands (Scheme 1b).[5] Complexes carrying ethacrynic acid and/or

flurbiprofen (*vide infra*) displayed marked cytotoxicity with respect to cisplatin in retinoblastoma and ovarian cancer cell lines, along with improved cancer cell selectivity.

In the light of these promising results, we decided to coordinate the bis-functionalized bipyridines to Ru(II) *p*-cymene and Ir(III) pentamethylcyclopentadienyl structures, which have been widely investigated for their anticancer potential.[6] Note that double functionalization with two different bio-fragments is quite rare for these metal scaffolds.[7] Four bioactive carboxylic acids were selected for the present work: *ethacrynic acid* (***E*-CO$_2$H**), *flurbiprofen* (***F*-CO$_2$H**), *biotin* (***B*-CO$_2$H**) and *benzylpenicillin* (***P*-CO$_2$H**) (Scheme 1c). Ethacrynic acid is an inhibitor of glutathione *S*-transferases (GST), enzymes that are implicated in resistance mechanism in various cancer cell lines.[2a,8] Ruthenium arene complexes derivatized with ethacrynic acid typically are cytotoxic also in cisplatin-resistant cell lines[9] whereas iridium-ethacrynic acid conjugates have not been reported yet. Cyclooxygenase enzymes (COX, especially COX-2) represent another important drug target as they are upregulated in several human cancers.[10] Thus a variety of nonsteroidal anti-inflammatory drugs – not including flurbiprofen – has been tethered to half sandwich ruthenium and iridium complexes (mostly Ru) to investigate their anticancer activity.[11] Biotin (vitamin B_{12}) has been frequently introduced in the structure of metal complexes aiming to assist their cellular uptake, taking advantage of the overexpression of vitamin receptors.[7b,12] In this regard, several biotinylated Ir(η^5-Cp*) derivatives have been investigated within the field of artificial metalloenzymes, but not in view of their possible anticancer activity.[13]

Benzylpenicillin was considered with a view to expand the panel of bioactive fragments of interest in the design of anticancer metal complexes. As a matter of fact, transition metal conjugates with β-lactam antibiotics (ampicillin, penicillin and related species) are sparse and have been mostly studied for their antibacterial activity.[14]

The cytotoxicity of herein reported hetero(bis)conjugated Ru and Ir complexes was investigated against ovarian, breast and cervical cancer cell lines, these cancers being currently treated using combination chemotherapy involving platinum and/or organic drugs.[15]

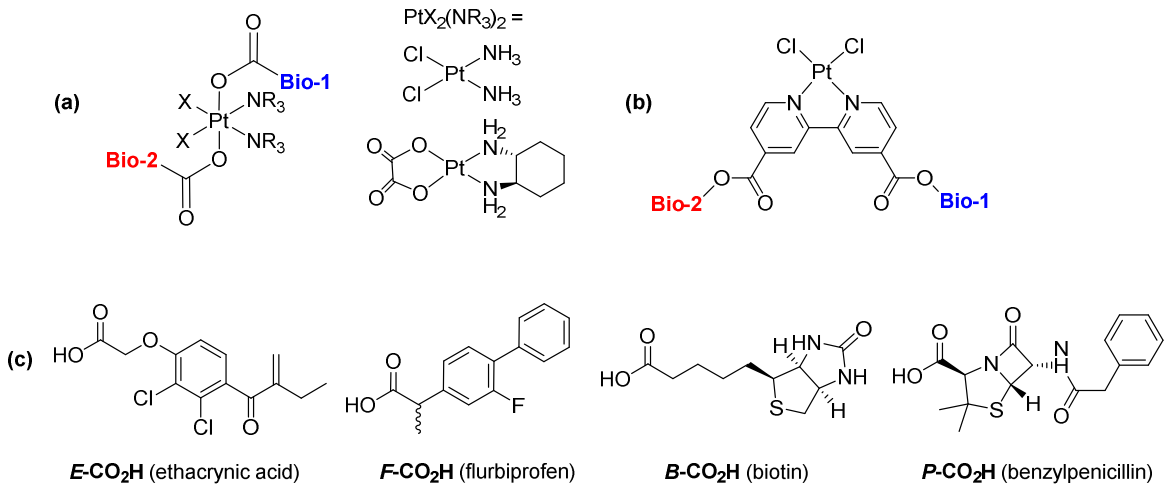

Scheme 1. General structure of platinum(IV) **(a)** and platinum(II) **(b)** complexes conjugated with two different bioactive molecules reported in the literature; bioactive carboxylic acids employed in this work **(c)**.

Results and discussion

1. Synthesis and characterization

Derivatization of 2,2′-bipyridine-4,4′-dicarboxylic acid with ethylene glycol followed by Steglich esterification/silica chromatography steps afforded the hetero-functionalized ligands containing ethacrynic acid and flurbiprofen ($\mathbf{L}^{EF}$) or biotin ($\mathbf{L}^{EB}$), according to the recently reported procedure (Scheme 2a).[5] A different strategy was adopted for the functionalization with benzylpenicillin, since a clean conversion of the commercially available potassium salt into the carboxylic acid was not effective. Thus, the bipyridine diacid was first converted into its 2-chloroethyl diester and then the latter was allowed to react with an excess of potassium benzylpenicillin in DMF at 85 °C, to afford the desired compound ($\mathbf{L}^{PP}$; Scheme 2b). Subsequently, treatment of $[RuCl_2(\eta^6\text{-}p\text{-cymene})]_2$ or $[IrCl_2(\eta^5\text{-}C_5Me_5)]_2$ with $AgNO_3$ in MeCN followed by reaction with the appropriate bipyridine ligand at reflux afforded complexes $[RuCl(\eta^6\text{-}p\text{-cymene})(\kappa^2N\text{-}\mathbf{L})]^+$ and $[IrCl(\eta^5\text{-}C_5Me_5)(\kappa^2N\text{-}\mathbf{L})]^+$, respectively ($\mathbf{L}^{EF}$: [**1-2**]$^+$; $\mathbf{L}^{EB}$: [**3-4**]$^+$; $\mathbf{L}^{PP}$: [**5**]$^+$, Scheme 2c). The reaction of bipyridine ligands ($\mathbf{L}^{EF}$, $\mathbf{L}^{EB}$) with the iridium dimer in chloroform under reflux and subsequent Cl^-/NO_3^- exchange was also effective (Scheme 2d). Dimethyl[2,2'-bipyridine]-4,4'-dicarboxylate ($\mathbf{L}^{MeMe}$) was synthesized according to a literature method[16]

and used to obtain [**6-7**]$^+$ as reference compounds. All reactions were carried out under stoichiometric conditions, and the Ru/Ir complexes were isolated as their nitrate salts in 83-95 % yield, without the needing for purification. The air- and moisture- stable ochre yellow (Ru) and orange (Ir) solids are soluble in polar organic solvents (e.g. DMSO, MeCN, CH_2Cl_2) but poorly soluble in water. To the best of our knowledge, the series of complexes [**1-5**]$^+$ includes the first cases of iridium and ruthenium compounds derivatized with flurbiprofen or benzylpenicillin[17] and also the first iridium-ethacrynic acid conjugate.

The novel compounds were characterized by analytical (CNH analysis), spectroscopic (solid-state IR, multinuclear and bidimensional NMR) and high-resolution MS spectrometry techniques (see Figures S1-S33 in the Supporting Information). In addition, the crystal structure of [**6**]BF_4 (obtained by [**6**]NO_3 + $NaBF_4$ metathesis) was confirmed by X-ray diffraction (see Figure S34/Table S1).[18]

The IR spectra of [**1-5**]NO_3 (in the solid state) display strong bands in the region 1760-1730 cm^{-1} accounting for the ester groups, along with other nearby C=O stretching absorptions. For instance, the bis-penicillin ester $\mathbf{L}^{PP}$ and the corresponding Ru(II) derivative [**5**]NO_3 show an additional intense band at 1780 cm^{-1} due to the β-lactam ring. The NMR spectra of [**1-4**]NO_3 contain two sets of signals, often overlapping; this effect is especially noticeable for $^1H/^{13}C$ NMR signals related to the bipyridine rings as well as in ^{19}F NMR spectra of [**1-2**]NO_3. Indeed, the asymmetry of bipyridine ligands $\mathbf{L}^{EB}$ and $\mathbf{L}^{EF}$ results in a chiral metal center and therefore complexes [**1-2**]$^+$ were obtained as a (racemic) mixture of diastereomers. On the other hand, [**5**]NO_3 exists as a single diastereomer, in which doubling of NMR signals is due to diastereotopic atoms (*e.g.* the CH protons of the *p*-cymene ligand). Accordingly, [**6-7**]NO_3 display symmetric, achiral bipyridine ligands giving rise to a single set of signals. The nitrate anion in [**1-7**]NO_3 manifests itself with a strong IR absorption around 1330 cm^{-1} and a ^{14}N NMR resonance occurring in the -1.5–3.5 ppm range.

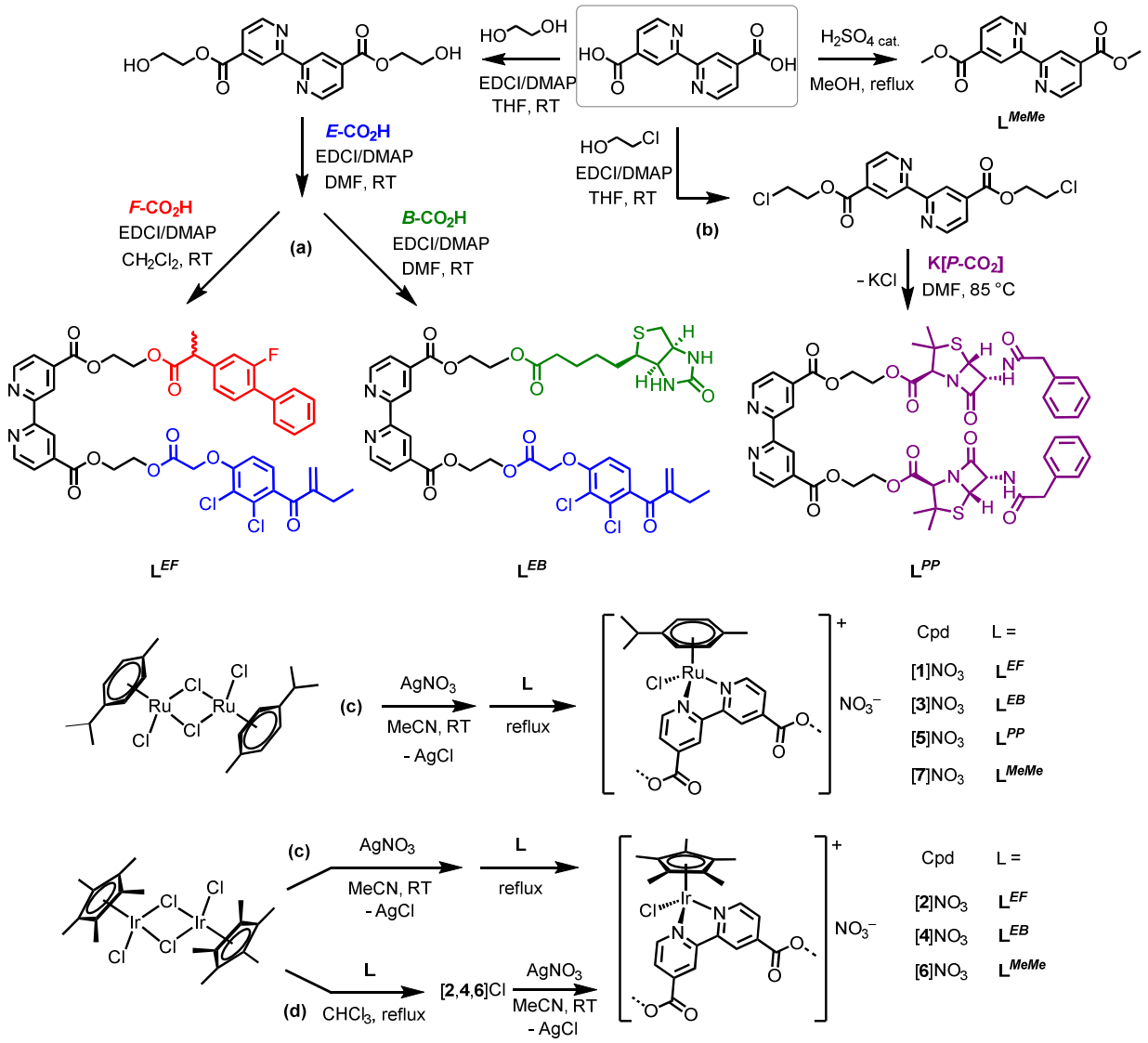

Scheme 2. Structures and synthetic routes for bipyridine ligands derivatized with ethacrynic acid (***E*-CO₂H**), flurbiprofen (***F*-CO₂H**), biotin (***B*-CO₂H**), benzylpenicillin (***P*-CO₂H**) and the respective ruthenium(II) *p*-cymene and iridium(III) pentamethylcyclopentadienyl complexes.

2. Behavior in aqueous solution and cell culture medium.

A preliminary assessment of the stability of ruthenium and iridium complexes in an aqueous medium[19] was carried out on 10 mM solutions in DMSO-d_6/D_2O 5:1 *v*/*v* at 37 °C by ^{1}H NMR. Under these conditions, all compounds were completely inert over 72 hours (≥ 96% stability; Figures S35-S39). Release of organic fragments, resulting from ligand dissociation and/or ester hydrolysis, was ruled out by comparison with the respective ^{1}H NMR spectra. Next, in order to check for metal-chloride solvolysis,

a stoichiometric amount of $Ag(CF_3SO_3)$ was added to $[\mathbf{6}]^+$ and $[\mathbf{7}]^+$. Partial or complete conversion of the starting material required heating at 50 °C for 3-5 hours (Figures S40-S41); spectral comparison before and after reaction with $Ag(CF_3SO_3)$ allowed unambiguous assignment of the set of signals to the parent chloro ($[\mathbf{6}]^+$, $[\mathbf{7}]^+$) and solvato ($[\mathbf{6^S}]^{2+}$, $[\mathbf{7^S}]^{2+}$) complexes (Scheme S1). Nevertheless, hydrolysis of M-Cl bonds on half-sandwich Ru(II) and Ir(III) 2,2'-bipyridine complexes should be facilitated on increasing dilution and water content of the medium.[20]

In contrast, transesterification processes are triggered upon dissolution in methanol at room temperature, as ascertained by NMR spectroscopy and MS spectrometry (see Experimental and Supporting Information). Such reactivity was previously observed for the bipyridines $\mathbf{L}^{EF}$ and $\mathbf{L}^{EB}$ and their Pt(II) complexes.[5] In the case of $[\mathbf{1\text{-}4}]^+$, methanolysis occurs predominantly at the bipyridine-bound carboxyl, leading to the release of 2-hydroxyethyl esters of the bioactive acids (*i.e.* ethacrynic acid, flurbiprofen, biotin). For comparison, the $\mathbf{L}^{MeMe}$ derivatives $[\mathbf{6\text{-}7}]^+$ are much more inert, indicating that the steric bulk of bioconjugated 2,2'-bipyridine ligands favors ester cleavage.

Next, the stability of ruthenium and iridium complexes under physiologically relevant conditions was investigated. Therefore 40 μM solutions of $[\mathbf{1\text{-}5}]NO_3$ in RPMI cell culture medium (1 % DMSO; pH ≈ 7.4) were incubated at 37 ° C for a variable time (0 / 24 / 48 h) then analyzed by HPLC-MS. The parent organometallic cation was recognized in solution in each case, along with fragments derived from hydrolysis of ester bonds. In this respect, the release of benzylpenicillin and the four 2-hydroxyethyl esters could not be quantified, due to matrix effects that have not been clarified. Conversely, the % amount of ethacrynic acid, biotin and flurbiprofen (carboxylates) released over time is reported in Table 1. Complexes $[\mathbf{1}]^+$ and $[\mathbf{2}]^+$ readily produce a minor amount (6-12 %) of ethacrynic acid, which decreases after 48 hours, possibly due to its degradation. No flurbiprofen was found in solution above the quantitation limit (0.4 μM) at any incubation time. A consistent amount of ethacrynic acid quickly detaches from both $[\mathbf{3}]^+$ and $[\mathbf{4}]^+$ (35-40 %) and more than a half of biotin was found in solution after 48 h. The aforementioned 2-hydroxyethyl esters might be biologically active themselves (*e.g.* in terms of

enzyme inhibition or anticancer activity[21]), or undergo a subsequent hydrolysis to release the bioactive carboxylate.

In conclusion, the stability experiments highlighted that Ru(II) and Ir(III) complexes [**1-5**]$^+$ possess a robust ligand set around the metal center, but are susceptible to ester hydrolysis in cell culture medium, leading to the progressive release of their bioactive organic cargo (in the form of carboxylates or 2-hydroxyethyl esters), thus behaving as pro-drugs. The timing of ester cleavage may affect their biological activity (*vide infra*).

Table 1. Percentage of ethacrynic acid, biotin and flurbiprofen carboxylates released from solutions of [**1-4**]$^+$ in RPMI cell culture medium (*ca*. 40 μM, 1 % DMSO, pH ≈ 7.4) at 37 °C for different incubation times (0 – 48 h).

Compound	% ***E*-CO_2H released** [a]			% ***F*-CO_2H or *B*-CO_2H released** [a][b]		
	0 h	**24 h**	**48 h**	**0 h**	**24 h**	**48 h**
[1]NO_3	6	4	3	0	0	0
[2]NO_3	12	14	8	0	0	0
[3]NO_3	34	33	28	9	29	51
[4]NO_3	39	28	26	10	40	64

[a] Starting concentrations of the complexes were in the range 33-41 μM. The analytical blank did not contain any relevant amount of the analytes. CV% was below 10%. [b] % ***F*-CO_2H** for [**1-2**]$^+$; % ***B*-CO_2H** for [**3-4**]$^+$.

3. Cytotoxicity, cellular uptake, DNA metalation and enzyme inhibition.

The antiproliferative activity of complexes [**1-7**]$^+$ was determined in four human cancer cell lines (A2780, A2780cisR ovarian ± cisplatin-resistant, MCF-7 breast and HeLa cervical) and non-tumorigenic human embryonic kidney cells (HEK293), following 72 h incubation. IC_{50} data are compiled in Table 2 with cisplatin, RAPTA-C, bipyridine ligands ($\mathbf{L}^{EF}$, $\mathbf{L}^{EB}$, $\mathbf{L}^{PP}$) and the bioactive carboxylic acids as reference compounds. Ethacrynic acid-derivatized compounds [**1-4**]$^+$ are potent cytotoxic agents in the panel of cell lines, with IC_{50} values ranging from 2.8 to 40 μM. The compounds are particularly effective on MCF-7 cells (compared to cisplatin) and on the cisplatin-resistant A2780cisR cell line, with resistance

factors below 2.2 (*vs*. 7 for cisplatin). Conversely, benzylpenicillin conjugates [**5**]NO_3 and $\mathbf{L}^{PP}$ are essentially non-toxic in all cell lines.

Interestingly, some cytotoxicity trends on varying the nature of the metal center (Ru/Ir) and the organic fragments can be delineated. First, each iridium complex ([**2**]$^+$/[**4**]$^+$/[**6**]$^+$) is slightly more cytotoxic than the respective ruthenium analogue ([**1**]$^+$/[**3**]$^+$/[**7**]$^+$). Second, flurbiprofen/ethacrynic acid conjugates ([**1-2**]$^+$) are more cytotoxic than their biotin/ethacrynic acid counterparts ([**3-4**]$^+$), while the opposite behavior is observed for the bipyridine ligands ($\mathbf{L}^{EF}$ being substantially non-cytotoxic while $\mathbf{L}^{EB}$ showing IC_{50}s comparable to the complexes). Third, cancer cell selectivity (*i.e.*, IC_{50} found for non-tumorigenic HEK293/IC_{50} found for the cancer cell line) increases on going from [**3**]$^+$/[**4**]$^+$ to [**1**]$^+$/[**2**]$^+$, peaking at *ca*. 4 for [**2**]NO_3 in A2780 cells. These trends hold for all the tested cell lines, remarking that the cytotoxic effect of [**1-4**]$^+$ is heavily influenced by the selection of metal center and bioactive fragments, and evidencing iridium/ethacrynic acid/flurbiprofen as the best combination. Notably, ruthenium and iridium bipyridine with simple methyl esters on the bipyridine ligand ([**6**]$^+$/[**7**]$^+$) are considerably less cytotoxic than the bis-conjugated derivatives [**1-4**]$^+$, suggesting that synergic effects are responsible for the biological activity of the latter. Note that incubation of a 1:1:1 mixture of flurbiprofen, ethacrynic acid and the Ru/Ir complex lacking bioactive fragments ([**6**]$^+$ and [**7**]$^+$) resulted in a 5- to 12-fold lower cytotoxicity with respect to the administration of a single compound ([**1**]$^+$ and [**2**]$^+$). The overall better performance of flurbiprofen/ethacrynic acid derivatives [**1-2**]$^+$, with respect to biotin/ethacrynic acid analogues [**3-4**]$^+$, may be in part related to a more controlled ester hydrolysis in the cellular environment (see above). It is noteworthy that biotinylated derivatives were not particularly effective also among bis-functionalized platinum(IV) complexes (Scheme 1a).[4a,g]

Table 2. IC_{50} values (μM) on human ovarian (A2780 and A2780cisR), breast (MCF-7) and cervical (HeLa) cancer cells, and human embryonic kidney (HEK-293) cells after 72 hours incubation. Values are given as the mean ± SD.

Compound(s)	Metal / bioactive fragments	A2780	A2780cisR	MCF-7	HeLa	HEK293
[1]NO_3	Ru / ethacrynic acid / flurbiprofen	5.6 ± 0.6	8.0 ± 0.7	10.6 ± 0.8	28 ± 4	7.3 ± 0.9

[2]NO_3	Ir / ethacrynic acid / flurbiprofen	2.8 ± 0.4	6.4 ± 0.5	8.0 ± 0.9	17.1 ± 0.6	10.3 ± 0.6
[3]NO_3	Ru / ethacrynic acid / biotin	11 ± 3	11 ± 2	22 ± 1	40 ± 6	9 ± 4
[4]NO_3	Ir / ethacrynic acid / biotin	7.0 ± 0.8	8.5 ± 0.5	9 ± 1	24 ± 5	12.5 ± 0.8
[5]NO_3	Ru / benzylpenicillin (x2)	> 200	> 200	270 ± 30	190 ± 10	> 200
[6]NO_3	Ir / −	>100	63 ± 6	140 ± 30	190 ± 9	> 100
[7]NO_3	Ru / −	>100	>100	310 ± 40	220 ± 20	> 100
L^{EF}	− / ethacrynic acid / flurbiprofen	> 200	> 200	> 200	> 200	> 200
L^{EB}	− / ethacrynic acid / biotin	12 ± 1	16 ± 1	17 ± 2	14 ± 2	25 ± 2
L^{PP}	− / benzylpenicillin (x2)	> 200	> 200	> 200	> 200	> 200
ethacrynic acid [a]		40 ± 3	53 ± 5	47 ± 4	56 ± 9	39 ± 1
flurbiprofen		> 200	> 200	190 ± 30	200 ± 50	> 200
benzylpenicillin [b]		> 200	> 200	> 200	> 200	> 200
[6]NO_3 + *E*-CO_2H + *F*-CO_2H [c]	Ir / ethacrynic acid / flurbiprofen	34 ± 2	35 ± 2	-	-	37 ± 3
[7]NO_3 + *E*-CO_2H + *F*-CO_2H [c]	Ru / ethacrynic acid / flurbiprofen	27 ± 3	39 ± 3	-	-	36 ± 2
cisplatin		2.1 ± 0.4	15 ± 1	14.8 ± 0.9	15 ± 3	5.3 ± 0.7
RAPTA-C [d]		> 200	> 200	-	-	> 200

[a] Data for A2780/A2780cisR and HEK293 taken from ref. 8c. [b] as K^+ salt. [c] Co-administration of the compounds in a 1:1:1 molar ratio. [d] [$RuCl_2(\eta^6$-*p*-cymene)(κ*P*-1,3,5-triaza-7-phosphaadamantane)].

In order to gain insights into the mode of action of the compounds, A2780 cells were incubated with 10 μM of [**1**-**7**]$^+$ for 8 and 24 h and 5 μM of [**1**-**7**]$^+$ for 24 h, and the metal content was determined by ICP-MS following established protocols (Table 3).[22] Cellular uptake for all tested compounds increases with incubation time and with concentration. Treatment with ethacrynic acid/flurbiprofen conjugates [**1**-**2**]$^+$ resulted in a substantially higher metal accumulation with respect to the non-functionalized reference complexes [**6**-**7**]$^+$. In contrast, biotin-functionalized complexes [**3**-**4**]$^+$ showed only a modest increase in cellular internalization, and the ruthenium content determined for the bis-penicillin [**5**]$^+$ or the bis-methyl [**7**]$^+$ esters was not significantly different. The DNA metalation level, following incubation with 10 μM of [**1**-**7**]$^+$ for 24 h, decreases in the sequence [**1**]$^+$ >> [**3**]$^+$ ≈ [**5**]$^+$ ≈ [**7**]$^+$ and [**2**]$^+$ >> [**4**]$^+$ > [**6**]$^+$ for Ru and Ir complexes, respectively, reflecting the amount of compound taken up by the cells in an almost linear fashion (Figure S45). Overall, these data correlate well with A2780 cytotoxicity, which is highest for compounds better internalized by the cells (*i.e.* [**1**]$^+$ and [**2**]$^+$).

Table 3. Cellular uptake of Ru or Ir from the investigated compounds in A2780 cells treated with 5 or 10 μM of [**1-7**]NO_3 for 8 or 24 h and DNA metalation in A2780 cells treated with 10 μM of [**1-7**]NO_3 for 24 h.

Compound	Metal / bioactive fragments	cellular uptake [pmol Ru(Ir)/10^6 cells]			DNA metalation
		10 μM/8h	5 μM/24h	10 μM/24h	fmol Ru(Ir)/μg DNA
[1]NO_3	Ru / ethacrynic acid / flurbiprofen	88 ± 7	65 ± 9	130 ± 9	52 ± 9 (21 ± 7) [a]
[2]NO_3	Ir / ethacrynic acid / flurbiprofen	61 ± 7	46 ± 6	100 ± 10	36 ± 3 (16 ± 3) [a]
[3]NO_3	Ru / ethacrynic acid / biotin	9 ± 1	7 ± 2	13 ± 4	5.0 ± 0.9
[4]NO_3	Ir / ethacrynic acid / biotin	11 ± 2	8 ± 2	17 ± 4	12 ± 2
[5]NO_3	Ru / benzylpenicillin (x2)	4.6 ± 0.9	3.2 ± 0.9	7 ± 1	4.8 ± 0.6
[6]NO_3	Ir / −	5 ± 1	5 ± 1	9.0 ± 0.7	8 ± 2
[7]NO_3	Ru / −	2.1 ± 0.3	4 ± 1	6.4 ± 0.9	4.2 ± 0.7

[a] In parentheses: DNA metalation with 5 μM [**1**]NO_3 and [**2**]NO_3 for 24 h.

To further explore whether DNA metalation plays a role in the cell-killing effect of the investigated compounds, we measured their antiproliferative activity in a pair of Chinese hamster ovary cell lines, CHO-K1 (wild-type) and its mutant cell line MMC-2. The latter is deficient in the DNA nucleotide excision repair (NER), thus the DNA damage in MMC-2 cells is more harmful than in the NER-proficient CHO-K1 cells. The degree of DNA damage involvement in the mechanism of action can be estimated from factor F, defined as the ratio of IC_{50} values estimated for CHO-K1 and MMC-2 cells. The four Ru/Ir bioconjugated complexes [**1-4**]$^+$ are slightly more efficient in the NER-deficient cell line MMC-2 than in the wild-type CHO-K1; this effect being more pronounced for the biotin derivatives [**3-4**]$^+$ than the flurbiprofen ones [**1-2**]$^+$ (Table 4 and Figure S46). The prominent involvement of DNA damage in cells treated with cisplatin is apparent, the compound being 9 times more active in the NER-deficient cells.

Table 4. Antiproliferative data (IC_{50} / μM)[a] for CHO-K1 (wild-type) and MMC-2 (NER-deficient) cells treated with [**1-4**]NO_3 and cisplatin. Values are given as mean ± SD.

Compound	CHO-K1	MMC-2	F [b]

[1]NO$_3$	23 ± 4	12.9 ± 0.3	1.8
[2]NO$_3$	18.9 ± 0.6	10.1 ± 0.2	1.9
[3]NO$_3$	29.0 ± 2	9.1 ± 0.7	3.2
[4]NO$_3$	25.7 ± 0.8	8.9 ± 0.2	2.9
cisplatin	29 ± 1	3.3 ± 0.1	8.8

[a] Determined by MTT assay after 72 h treatment. [b] Defined as IC_{50} (NER efficient)/IC_{50} (NER deficient)

Next, we performed cell viability studies of [**1-4**]$^+$ and cisplatin in A2780 cells using the MTT assay with variable treatment time (24/48/72 h; Table 5). The effect of DNA metalation resulting in DNA damage is usually related to inhibition of DNA replication or transcription, which only becomes apparent after a longer time of the treatment (after at least one cell cycle is completed). Cisplatin is a typical example of this behavior, whose mechanism of action is primarily related to its ability to modify DNA and its cytotoxicity is strongly time-dependent. Indeed, the IC_{50} values obtained for cisplatin after 24 h were markedly higher (9 times) than those determined after 72 h treatment. Conversely, we observed almost no variation of the IC_{50} values along the treatment time (except for [**3**]NO_3 at 24 h). Thus, it seems reasonable to suggest that the cytotoxic effects of [**1-4**]$^+$ might contribute to the overall cell growth inhibition more than their antiproliferative effects. In accordance with the antiproliferative activity in cell lines proficient and deficient in NER (Table 4), these results support the view that DNA metalation might be involved in the mechanism of action of [**1-4**]$^+$, although other routes are likely to play a more significant role.

Table 5. Time-dependent cytotoxicity expressed in IC_{50} (μM) of four active compounds in A2780 cells. The values are given as mean ± SD.

Compound	IC_{50} / μM		
	24 h	**48 h**	**72 h**
[1]NO$_3$	6.7 ± 0.2	6.1 ± 0.3	5.6 ± 0.3
[2]NO$_3$	3.0 ± 0.1	2.9 ± 0.1	2.8 ± 0.1
[3]NO$_3$	20 ± 2	12.7 ± 0.2	11.1 ± 0.4
[4]NO$_3$	8 ± 1	7.6 ± 0.8	7.0 ± 0.8
cisplatin	34 ± 4	4.9 ± 0.9	3.6 ± 0.7

In this respect, we performed experiments to assess whether the ethacrynic acid/flurbiprofen derivatized complexes [**1-2**]$^+$ are able to affect glutathione S-transferase (GST) and cyclooxygenase (COX) activity. Thus, lysates of the HeLa cells treated for 18 h with [**1**]NO_3 and [**2**]NO_3 at concentrations corresponding to their respective IC_{50} values (determined with MTT after 72 h; Table 2), were prepared and analyzed with either Glutathione S-Transferase Fluorescent Activity Kit (Invitrogen^{TM}) or Cyclooxygenase Activity Kit (Fluorimetric) (Abcam). Similarly, combinations of the non-functionalized complexes [**6**]$^+$/[**7**]$^+$ with the reference enzyme inhibitors (***F*-CO$_2$H** / ***E*-CO$_2$H**) or the bipyridine ligand $\mathbf{L}^{EF}$ at identical concentrations were tested. Results are shown in Figures 1 and S47, showing that GST activity was significantly reduced in the cells treated with both ethacrynic acid carrying compounds [**1**]NO_3 and [**2**]NO_3, as well as in the cells treated with the mixtures containing ***E*-CO$_2$H**. Nevertheless, [**1**]NO_3 and [**2**]NO_3 caused a stronger inhibition, reducing the enzyme activity to 68 and 62 %, respectively. No significant inhibition of COX activity was observed, except for [**2**]NO_3.

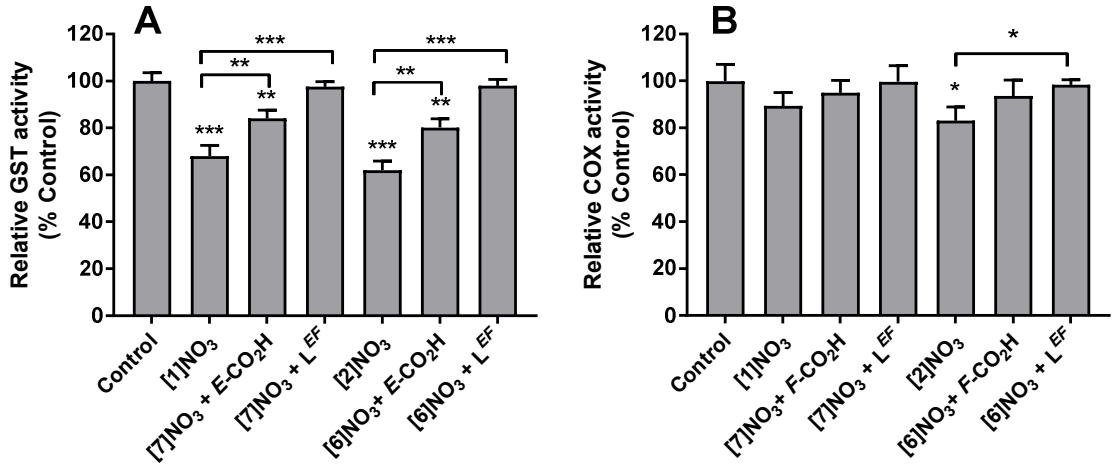

Figure 1. The effect of the tested compounds on GST (A) and COX (B) activity in HeLa cells. The cells were incubated with [**1**]NO_3 and [**2**]NO_3 at the concentrations corresponding to their respective IC_{50} values (72 h; MTT) for 18 h. For comparison, the cells were also treated with combinations of [**7**]NO_3 or [**6**]NO_3 with ***E*-CO$_2$H** (A) and ***F*-CO$_2$H** (B) or with $\mathbf{L}^{EF}$ at concentrations identical to [**1**]NO_3 or [**2**]NO_3, respectively. The enzyme activities are expressed in % of enzyme activities in non-treated control cells. The GST activity was determined with Glutathione S-Transferase Fluorescent Activity Kit (Invitrogen^{TM}). The COX activity was determined with Cyclooxygenase

Activity Assay Kit (Fluorimetric) (Abcam). Statistical analysis was performed using Student´s t-test. Statistically significant differences from non-treated control are shown above individual bars; statistically, significant differences between samples are given above the brackets (*p≤0.05; **p≤0.01 and ***p≤0.001).

In conclusion, the mechanism of action of the investigated compounds [**1-4**]$^+$ is likely multimodal, involving DNA metalation as well as enzyme inhibition. However, the cytotoxic effects associated to the enzyme inhibition activity possibly outweigh the effects caused by DNA metalation.

Enzyme inhibition by [**1**]$^+$ and [**2**]$^+$ could be enacted by metal-based species (*e.g.* the organometallic cations) or by the bioactive organic fragments that are released upon entering the cell. Judging from the stability studies in cell culture medium and the metal uptake experiments (*see above*), it is apparent that both the internalization of the compounds as well as the release of the bioactive groups from the respective Ir or Ru complexes are time-dependent. Nevertheless, the fact that cytotoxicity does not increase from 24 to 72 h (Table 5) points out that these compounds mostly exert their biological activity within the first 24 h of the treatment.

Conclusions

Ruthenium(II) arene and iridium(III) cyclopentadienyl complexes are amongst the most investigated transition metal compounds in the landscape of the development of new anticancer drugs able to overcome the limitations associated with the use of platinum chemotherapeutics. In addition, the conjugation with suitable bioactive fragments is an intriguing and well-established strategy aimed to improve the anticancer activity of a metal complex. Remarkably, the bis-functionalization of metal complexes with two different bioactive molecules appears to be an even more promising approach which has been successfully investigated on platinum(IV) complexes, but its applicability to other metal structures remains undeveloped, possibly due to the lack of adequate synthetic routes. Here, we have employed a commercial bipyridine as a convenient starting material to obtain new half sandwich Ru(II)

and Ir(III) complexes doubly functionalized with different bioactive carboxylic acids, including hetero-functionalized derivatives. The complexes manifest a stable coordination environment and a variable tendency to release the bioactive molecules in aqueous media. Biological experiments on ovarian, breast and cervical cancer cell lines revealed an improved cytotoxicity profile for both Ru(II) and Ir(III) complexes, with ethacrynic acid / flurbiprofen as the most effective combination. The activity of the compounds is associated to an increased cellular uptake, DNA metalation, and COX/GST enzyme inhibition. The latter is possibly related to the bioactive carboxylic acids (or their derivatives) that are released by hydrolysis. Synergic effects on cytotoxicity and enzyme inhibition were clearly observed by control combination experiments. The efficacy of the proposed method strongly encourages further studies aimed to identify other combinations of bioactive molecules and may be easily extended to other metal scaffolds investigated for pharmacological activity.

Experimental

1. General experimental details

$RuCl_3 \cdot xH_2O$ (41.9 % Ru; Chimet S.p.A), $IrCl_3 \cdot xH_2O$ (59.9 % Ir; Merck) and other chemicals (≥ 99% purity) were purchased from Alfa Aesar, Merck, Apollo Scientific or TCI Chemicals. Ethacrynic acid (***E*-CO₂H**),[23] flurbiprofen (***F*-CO₂H**),[23] biotin (***B*-CO₂H**),[23] potassium benzylpenicillin (K[***P*-CO₂**]),[23] 2,2′-bipyridine-4,4′-dicarboxylic acid and ethyl(diisopropylamino)carboxydiimide hydrochloride (EDCI·HCl; at – 20 °C) were stored under N_2 as received. Ethylene glycol was dried under high vacuum over P_2O_5 and stored under N_2. Column chromatography was carried out with silica gel (70-230 mesh). $[RuCl_2(\eta^6\text{-}p\text{-cymene})]_2$,[24] $[IrCl_2(\eta^5\text{-}C_5Me_5)]_2$,[25] and bipyridine ligands[5] $\mathbf{L}^{EF}$ and $\mathbf{L}^{EB}$ were synthesized according to literature methods. All operations were carried out in air with common laboratory glassware, except the syntheses of bioconjugated bipyridine ligands, [**2**]Cl and [**4**]Cl that were carried out under N_2 using standard Schlenk techniques and solvents distilled from appropriate drying agents (DMF from BaO, THF from CaH_2, CH_2Cl_2 and $CHCl_3$ from P_2O_5). Once isolated, organic bipyridine esters were

stored at 4 °C; all Ru and Ir compounds were air- and moisture-stable in the solid state at room temperature. NMR spectra were recorded at 25 °C on a Bruker Avance II DRX400 instrument equipped with a BBFO broadband probe. Chemical shifts (in ppm) are referenced to the residual solvent peaks[26] (^{1}H, ^{13}C) or to external standards[27] (^{14}N to CH_3NO_2, ^{19}F to $CFCl_3$, ^{35}Cl to 1 M NaCl in D_2O). ^{1}H and ^{13}C spectra were assigned with the aid of ^{13}C DEPT 135, ^{1}H-^{1}H COSY, ^{1}H-^{13}C *gs*-HSQC and ^{1}H-^{13}C *gs*-HMBC experiments.[28] $CDCl_3$ for NMR analysis was stored in the dark over Na_2CO_3. IR spectra (650-4000 cm^{-1}) were recorded on a Perkin Elmer Spectrum One FT-IR spectrometer, equipped with a UATR sampling accessory and processed with Spectragryph software.[29] CHNS analyses were performed on a Vario MICRO cube instrument (Elementar). ESI-Q/ToF flow injection analyses (FIA) were conducted on a 1200 Infinity HPLC coupled to a Jet Stream ESI interface with a Quadrupole-Time of Flight tandem mass spectrometer 6530 Infinity Q-TOF (Agilent Technologies, USA). HPLC-MS grade acetonitrile was used as mobile phase (Carlo Erba, Italy). The flow rate was 0.2 mL/min (total run time 3 min), the injection volume 3 μL. ESI operating conditions: drying gas (N_2, purity > 98%), 350 °C and 10 L/min; capillary voltage 4.5 KV; nozzle voltage: 1 KV; nebuliser gas 35 psig; sheath gas (N_2, purity > 98%): 375 °C and 11 L/min. The fragmentor was kept at 50 V, the skimmer at 65 V and the OCT 1 RF at 750 V. High resolution MS and MS/MS spectra were achieved in positive mode in the range 100-1700 m/z; the mass axis was routinely calibrated using the tuning mix HP0321 (Agilent Technologies) prepared in acetonitrile and water. Prior to injection, each sample was properly diluted to c.a. 20 μg/g. Analytical, spectroscopic and spectrometric characterization of compounds is given in the Supporting Information.

2. Synthesis of compounds

Bis(2-chloroethyl)[2,2'-bipyridine]-4,4'-dicarboxylate (Chart 1).

In a 50-mL Schlenk tube under N_2, 2,2′-bipyridine-4,4′-dicarboxylic acid (529 mg, 2.17 mmol), DMAP (65 mg, 0.57 mmol), EDCI·HCl (992 mg, 5.17 mmol), THF (12 mL) and 2-chloroethanol (0.30 mL, 4.47 mmol) were introduced in this order. The milky colourless suspension was stirred at room temperature

overnight, affording a colourless solution and a pink solid. Volatiles were removed under vacuum; the residue was suspended in CH_2Cl_2 and moved on top of a silica column (h 4, d 3.5 cm). Impurities were eluted with CH_2Cl_2 (40 mL) and the title compound was eluted with a CH_2Cl_2/hexane/acetone 10:5:2 *v/v/v* mixture (85 mL). Following removal of the volatiles under vacuum (40 °C), the resulting colourless solid was dried under vacuum (RT over P_2O_5) then stored under N_2. Yield: 465 mg, 58 %.

Chart 1. Structure of bis(2-chloroethyl)[2,2'-bipyridine]-4,4'-dicarboxylate.

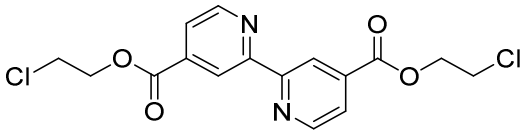

Bis(2-benzylpenicillinyloxyethyl)[2,2'-bipyridine]-4,4'-dicarboxylate, L^{PP} (Chart 2).

In a 50-mL Schlenk tube under N_2, bis(2-chloroethyl)[2,2'-bipyridine]-4,4'-dicarboxylate (202 mg, 0.546 mmol), K[***P*-CO₂**] (544 mg, 1.46 mmol) and DMF (8 mL) were introduced. The suspension (colourless solution + solid) was stirred at 85 °C for 18 h. The conversion was checked by ^{1}H NMR ($CDCl_3$) then the brown suspension was cooled to room temperature and volatiles were removed under vacuum. The residue was suspended in acetone and filtered over a short silica pad. The filtrate was taken to dryness under vacuum; the residue was dissolved in CH_2Cl_2 and moved on top of a silica column (h 6, d 2.5 cm). Impurities were eluted with CH_2Cl_2 and the title compound was eluted with CH_2Cl_2/acetone (7:1 to 3:1 *v/v* gradient). Following removal of the volatiles under vacuum, the resulting pale yellow foamy solid was dried under vacuum (RT over P_2O_5) then stored at 4 °C. Yield: 201 mg, 37 %.

Chart 2. Structure of L^{PP}.

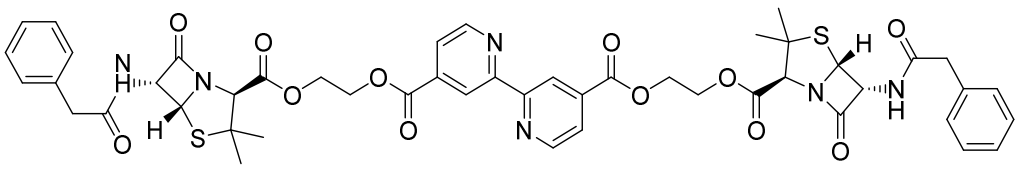

Synthesis of Ru and Ir compounds

Method A. A solution of $[RuCl_2(\eta^6\text{-}p\text{-cymene})]_2$ or $[IrCl_2(\eta^5\text{-}C_5Me_5)]_2$ (20-50 mg) in MeCN (2 mL) was treated with $AgNO_3$ (2.0 equivalents) and stirred at room temperature in the dark. After 1 h, the suspension (yellow/orange solution + colourless solid) was filtered over a celite pad. The selected bipyridine ligand (2.0 equivalents) was added to the filtrate and the mixure was stirred at reflux for 1-2 h. Next, the conversion was checked by NMR (^1H $CDCl_3$) and volatiles were removed under vacuum. The residue was dissolved in CH_2Cl_2 and the solution was filtered through celite. The filtrate was dried under vacuum; the resulting ochre yellow (Ru) or orange (Ir) solid was washed with Et_2O and dried under vacuum (40 °C).

Method B *(Ir compounds).* In a 25 mL Schlenk tube, a solution of $[IrCl_2(\eta^5\text{-}C_5Me_5)]_2$ (*ca*. 25 mg) and the selected bipyridine (2.0 equivalents) in $CHCl_3$ (8 mL) was stirred at reflux for 14 h. The resulting orange solution was taken to dryness under vacuum and the residue was triturated in Et_2O. The suspension was filtered; the orange solid, namely $[IrCl(\eta^5\text{-}C_5Me_5)(\text{bipyridine})]Cl$, was washed with Et_2O and dried under vacuum (40 °C). Subsequently, a fraction of the Ir compound (*ca.* 60 mg) was dissolved in MeCN (2 mL) and treated with $AgNO_3$ (1.0 equivalent). The suspension was stirred at room temperature in the dark for 4 h. Next, the mixture (orange solution + colourless solid) was filtered over a celite pad and the filtrate was taken to dryness under vacuum. The residue was dissolved in CH_2Cl_2 and filtered again through celite. The filtrate was dried under vacuum; the resulting orange solid was washed with Et_2O and dried under vacuum (40 °C).

<u>*Note*</u>: the use of methanol as an alternative solvent for the synthesis and/or workup is NOT recommended, due to transesterification processes (*vide infra*).[30]

$[RuCl(\eta^6\text{-}p\text{-cymene})(\kappa^2N\text{-}L^{EF})]NO_3$, [1]$NO_3$ (Chart 3). Prepared using $[RuCl_2(\eta^6\text{-}p\text{-cymene})]_2$ (30 mg, 0.05 mmol), $AgNO_3$ (17 mg, 0.10 mmol) and $\mathbf{L}^{EF}$ (86 mg, 0.10 mmol), according to method **A**. Yield: 102 mg, 88 %.

Chart 3. Structure of [**1**]$^+$.

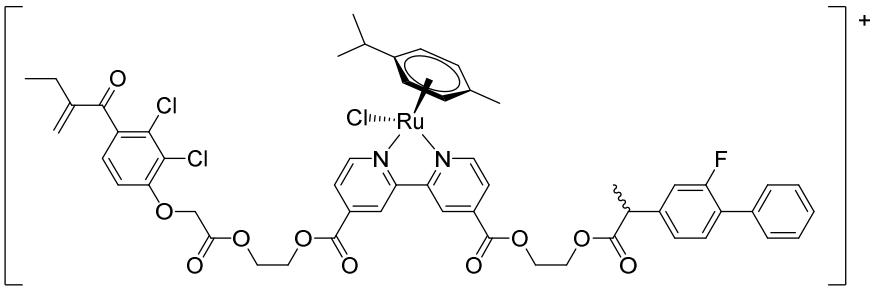

[IrCl(η^5-C$_5$Me$_5$)(κ^2*N*-L^{EF})]$^+$, [2]$^+$ (Chart 4). [2]Cl. Prepared using [IrCl$_2$(η^5-C$_5$Me$_5$)]$_2$ (26 mg, 0.033 mmol), and **L^{EF}** (58 mg, 0.069 mmol), according to method **B**. Yield: 79 mg, 98 %. **[2]NO$_3$.** Prepared using [IrCl$_2$(η^5-C$_5$Me$_5$)]$_2$ (35 mg, 0.045 mmol), AgNO$_3$ (15 mg, 0.088 mmol) and **L^{EF}** (76 mg, 0.089 mmol), according to method **A**. Yield: 104 mg, 93 %. Alternative preparation from [**2**]Cl (79 mg, 0.064 mmol) and AgNO$_3$ (11 mg, 0.064 mmol), following method **B**. Yield: 67 mg, 83 %.

Chart 4. Structure of [**2**]$^+$.

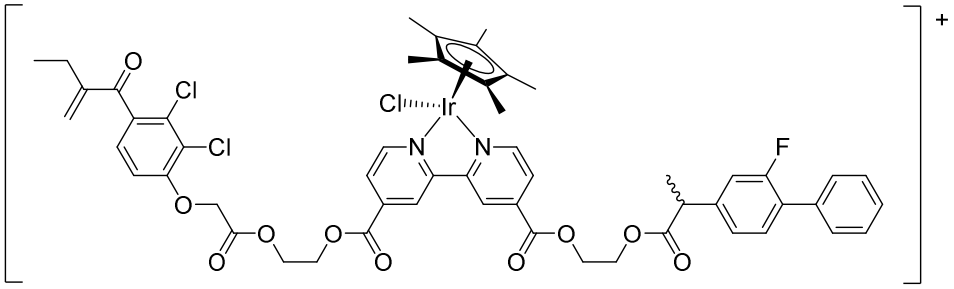

[RuCl(η^6-*p*-cymene)(κ^2*N*-L^{EB})]NO$_3$, [3]NO$_3$ (Chart 5). Prepared using [RuCl$_2$(η^6-*p*-cymene)]$_2$ (30 mg, 0.05 mmol), AgNO$_3$ (17 mg, 0.10 mmol) and **L^{EB}** (84 mg, 0.10 mmol), according to method **A**. Yield: 109 mg, 95 %.

Chart 5. Structure of [**3**]$^+$.

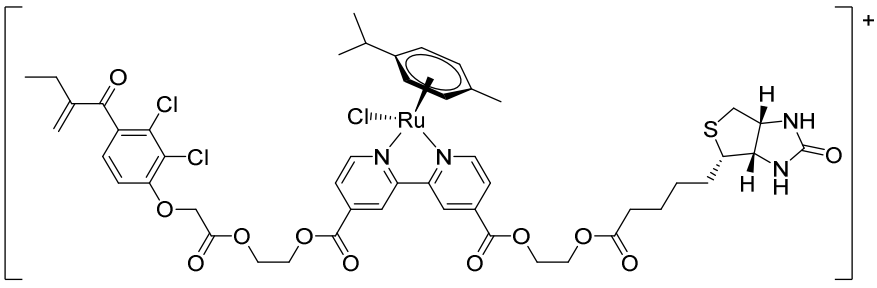

[IrCl(η^5-C$_5$Me$_5$)(κ^2*N*-L^{EB})]$^+$, [4]$^+$ (Chart 6). [4]Cl. Prepared using [IrCl$_2$(η^5-C$_5$Me$_5$)]$_2$ (27 mg, 0.034 mmol), and **L^{EB}** (58 mg, 0.067 mmol), according to method **B**. Yield: 78 mg, 94 %. **[4]NO$_3$.** Prepared using [IrCl$_2$(η^5-C$_5$Me$_5$)]$_2$ (36 mg, 0.045 mmol), AgNO$_3$ (16 mg, 0.091 mmol) and **L^{EB}** (77 mg, 0.091 mmol), according to method **A**. Yield: 110 mg, 95 %. Alternative preparation from [**4**]Cl (60 mg, 0.048 mmol) and AgNO$_3$ (9 mg, 0.053 mmol), following method **B**. Yield: 51 mg, 83 %.

Chart 6. Structure of [**4**]$^+$.

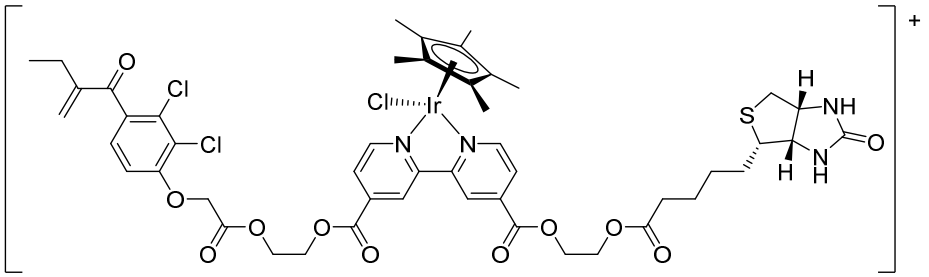

[RuCl(η^6-*p*-cymene)(κ^2*N*-L^{PP})]NO$_3$, [5]NO$_3$ (Chart 7). Prepared using [RuCl$_2$(η^6-*p*-cymene)]$_2$ (17 mg, 0.028 mmol), AgNO$_3$ (10 mg, 0.059 mmol) and **L^{PP}** (55 mg, 0.057 mmol), according to method **A**. Yield: 68 mg, 94 %.

Chart 7. Structure of [**5**]$^+$.

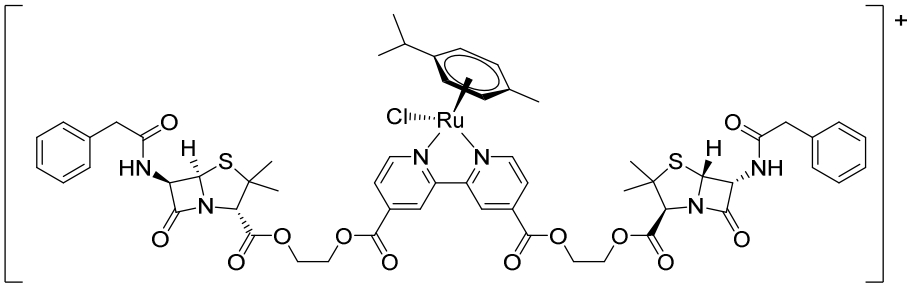

Dimethyl[2,2'-bipyridine]-4,4'-dicarboxylate, L^{MeMe} (Chart 8). The title compound was prepared according to a modified literature procedure.[16] In a 100 mL round bottom flask, 98% H$_2$SO$_4$ (1.6 mL, 30 mmol) was added dropwise to a suspension of 2,2′-bipyridine-4,4′-dicarboxylic acid (502 mg, 2.06 mmol) in MeOH (30 mL). The mixture was stirred at reflux for 29 h. The resulting pink solution was

cooled to room temperature and NaOH (1 M in water, 30 mL, 30 mmol) was added dropwise. Subsequently, MeOH was removed under reduced pressure and the mixture (pink aqueous solution + colourless precipitate) was extracted with CH_2Cl_2 (3 x 40 mL). The combined organic extracts were filtered through a celite pad and dried under vacuum. The resulting colourless solid was washed with Et_2O and dried under vacuum (40°C). Yield: 509 mg, 91 %.

Chart 8. Structure of $\mathbf{L}^{MeMe}$.

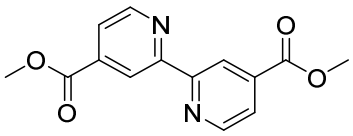

$[IrCl(\eta^5\text{-}C_5Me_5)(\kappa^2N\text{-}L^{MeMe})]X$, [6]X (X = NO_3, BF_4) (Chart 9). Synthesis of the related compound [**6**]Cl from $[IrCl_2(\eta^5\text{-}C_5Me_5)]_2$/$\mathbf{L}^{MeMe}$ was previously reported.[18] **[6]NO_3**. Prepared using $[IrCl_2(\eta^5\text{-}C_5Me_5)]_2$ (36 mg, 0.069 mmol), $AgNO_3$ (24 mg, 0.14 mmol) and $\mathbf{L}^{MeMe}$ (38 mg, 0.14 mmol), according to method **A**. Yield: 85 mg, 83 %. **[6]BF_4.** Compound [**6**]NO_3 (51 mg, 0.073 mmol) was dissolved in acetone (5 mL) and treated with $NaBF_4$ (11 mg, 0.10 mmol). The mixture was heated at reflux for 4 h then taken to dryness under vacuum. The residue was suspended in CH_2Cl_2 and filtered through a celite pad, in order to remove $NaNO_3$. The filtrate was taken to dryness under vacuum and dissolved in MeOH (*ca.* 3 mL). The solution was heated to reflux then allowed to cool down to room temperature. The resulting bright orange crystalline solid was collected by filtration, washed with Et_2O and dried under vacuum (40 °C). Yield: 47 mg, 89 %. X-ray quality crystals of [**6**]BF_4 were obtained from a MeCN solution layered with Et_2O and settled aside at – 20 °C (Table S1, Figure S34).

Chart 9. Structure of $[\mathbf{6}]^+$.

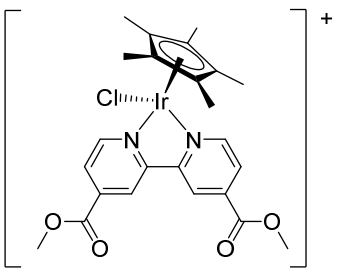

[RuCl(η^6-*p*-cymene)(κ^2*N*-L^{MeMe})]NO$_3$, [7]NO$_3$ (Chart 10). Prepared using [RuCl$_2$(η^6-*p*-cymene)]$_2$ (57 mg, 0.093 mmol), AgNO$_3$ (32 mg, 0.19 mmol) and **L^{MeMe}** (51 mg, 0.19 mmol), according to method **A**. Yield: 107 mg, 96 %.

Chart 10. Structure of [**7**]$^+$.

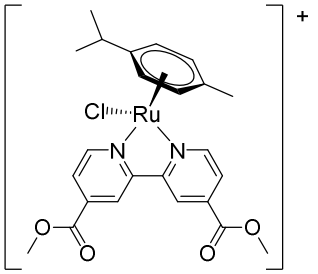

3. X-Ray crystallography

XRD experiments were performed using Mo–Kα radiation on a Bruker APEX II diffractometer equipped with a PHOTON2 detector. Data were corrected for Lorentz polarization and absorption effects (empirical absorption correction SADABS).[31] The structure was solved by direct methods and refined by full-matrix least-squares based on all data using F^2.[32] H atoms were fixed at calculated positions and refined by a riding model. Non hydrogen atoms were refined with anisotropic displacement parameters. Crystal data and collection details for [**6**]BF$_4$ are reported in Table S1.

4. Solution stability studies

Stability in DMSO/water. The selected Ru or Ir compound ($1.0 \cdot 10^{-2}$ M for [**1-5**]NO$_3$; $2 \cdot 10^{-2}$ M for [**6-7**]NO$_3$) was dissolved in a DMSO-d$_6$/D$_2$O 5:1 *v*/*v* solution (0.6 mL) containing dimethyl sulfone (Me$_2$SO$_2$, $5 \cdot 10^{-3}$ M) as internal standard for ^{1}H NMR[33] (δ = 2.96 ppm (s, 6H) in DMSO-d$_6$/D$_2$O 5:1). A single set of ^{1}H and ^{19}F{^{1}H} NMR signals was observed for the freshly-prepared yellow (Ir) or orange (Ru) solution, attributed to the starting material. Next, the solution was heated at 37 °C for 72 h and NMR analyses were repeated (Figures S35-S41). The % amount of starting material in solution with respect to

the initial spectrum, falling in the 96–98 % range for all compounds, was calculated by ^{1}H NMR integration with respect to Me_2SO_2 as internal standard. NMR data for the tested compounds are reported in the SI (DMSO-d_6/D_2O 5:1 *v*/*v* solutions); chemical shifts are referenced to the residual peak as in pure DMSO-d_6 (δ/ppm = 2.50).

Chloride/solvent exchange in DMSO/water. The DMSO-d_6/D_2O 5:1 *v*/*v* solution of [**6**]NO_3 or [**7**]NO_3 (0.5 mL; $2{\cdot}10^{-2}$ M) was maintained at 37 °C up to 86 h, then analyzed by ^{14}N and ^{35}Cl NMR (2000 scans).[34] Subsequently, Ag(CF_3SO_3) was added (0.10 mL of a 0.12 M solution in DMSO-d_6/D_2O 2:1 *v*/*v*; 1.2 equivalents) and the NMR tube was kept in the dark at 50 °C for 5 h, affording an orange (Ru) or yellow (Ir) solution and a colourless precipitate (AgCl). The solid was separated and ^{1}H, ^{14}N and $^{19}F\{^{1}H\}$ NMR spectra were recorded. Complete ([**6**]$^{+}$) or partial ([**7**]$^{+}$, ≈ 50%) conversion of the starting material was observed in the ^{1}H NMR spectrum (Figure S40-S41). The new set of signals, low-field shifted with respect to the starting metal-chlorido species, was attributed to the solvato-species [Ir(η^5-C_5Me_5)(**L**^{MeMe})(*solv*)]$^{2+}$, [**6**^{S}]$^{2+}$ and [Ru(η^6-*p*-cymene)(**L**^{MeMe})(*solv*)]$^{2+}$, [**7**^{S}]$^{2+}$ (*solv* = D_2O, DMSO-d_6; Scheme S1). No solvolysis of metal-chloride bonds occurred before Ag(CF_3SO_3) addition, as indicated by the absence of a ^{35}Cl NMR signal and comparison with ^{1}H NMR data for the solvato-species [**6**^{S}]$^{2+}$ and [**7**^{S}]$^{2+}$.

Stability in methanol. A freshly-prepared solution of the selected compound in CD_3OD (0.6 mL; $5{\cdot}10^{-3}$ M) was analyzed by ^{1}H and $^{19}F\{^{1}H\}$ NMR. Next the orange (Ru) or yellow/orange (Ir) solution was maintained at room temperature (≈ 25 °C) and periodically analysed by ^{1}H and $^{19}F\{^{1}H\}$ NMR. Once equilibrium was reached (no further change observed in NMR spectra), 1D and 2D NMR experiments (^{1}H, ^{13}C, ^{19}F, ^{14}N, ^{13}C-DEPT 135, ^{1}H-^{1}H COSY, ^{1}H-^{13}C *gs*-HSQC, ^{1}H-^{13}C *gs*-HMBC) were performed for a complete spectral assignment. The identity of compounds in solution (Schemes S2-S7) was checked by comparison with NMR data of pure compounds and by ESI-MS(+) spectrometry on CH_3OH solutions in the case of [**3**]$^{+}$ and [**4**]$^{+}$. The (%) relative amount of compounds in solution was calculated by ^{1}H

NMR integration. Experimental details, MS and NMR data (CH_3OH and CD_3OD, respectively) for the tested compounds are reported in the SI (Figures S42-S44; Tables S2-S4).

Stability in the cell culture medium. A stock solution of the selected Ru/Ir compound (*ca*. $3 \cdot 10^{-3}$ mmol/g) was prepared in DMSO and stored at room temperature. RPMI 1640 cell culture medium (Sigma Aldrich) was treated with NaH_2PO_4 / Na_2HPO_4 (c_{PO4} = 190 mM, pH = 7.35) then stored at 4 °C under N_2. In three 2 mL vials, the stock solution (20 µL) was added to the cell culture medium (2.0 mL) and the final mixtures (Ru/Ir *ca*. 45 µmol/g, 1 % DMSO) were heated at 37 °C for different times (0 / 24 / 48 h) under stirring. A fourth reference solution was prepared by adding the stock solution (20 µL) to HPLC water (2.0 mL). Next, the solutions were filtered on PTFE syringe filters, 0.45 µm, and analyzed by HPLC/ESI(+)-MS. LC separation was conducted on an analytical reversed-phase Poroshell 120 EC-C18 column (3.0 x 75 mm, particle size 2.7 µm; Agilent Technologies) with a Zorbax pre-column (4.6 x 12.5 mm, particle size 5 µm; Agilent Technologies) at 30 °C. The separation was achieved using a gradient of formic acid (FA) 0.1 % *v/v* in H_2O (eluent A) and FA 0.1% v/v in CH_3CN (eluent B), both LC-MS grade; the flow rate was 0.4 mL/min and the injection volume was 4 µL. The elution program started from 95% A, hold for 2.6 minutes, then linear gradient to 50% B in 13 minutes, then to 70% B in 5 minutes and then to 100% B in 6 minutes, held for 5 minutes. Re-equilibration took 5 minutes. ESI operating conditions: *drying gas* (N_2, purity >98%): 350 °C and 10 L/min; *capillary voltage* 4.5 KV; nozzle voltage: 1 KV; *nebuliser gas* 35 psig; *sheath gas* (N_2, purity >98%): 375 °C and 11 L/min. The fragmentor was at 175 V, the skimmer at 65 V and the OCT 1 RF at 750 V. High resolution MS spectra were achieved from 5 minutes to 30 minutes in positive mode in the range 100-1700 m/z; the mass axis was calibrated daily using the Agilent tuning mix HP0321 (Agilent Technologies) prepared in acetonitrile and water. Calibration curves for ***E*-CO_2H**, ***B*-CO_2H** and ***F*-CO_2H** were derived in the 0.4-10 µM range from stock solutions containing the three analytes *ca*. 80 µmol/g in water, appropriately diluted in HPLC grade water.

5. Biological studies

Cytotoxicity. Human ovarian carcinoma (A2780 and A2780cisR) cell lines were obtained from the European Collection of Cell Cultures. The human embryonic kidney (HEK-293) cell line was obtained from ATCC (Merck, Buchs, Switzerland). The human cervical carcinoma HeLa cells and human breast cancer MCF-7 cells were purchased from the European Collection of Authenticated Cell Cultures (ECACC) (Salisbury, UK). Chinese hamster ovary CHO-K1 cell line (wild type) and its derivative MMC-2 carrying the ERCC3/XPB mutation (NER-deficient) cell line were kindly supplied by Dr. M. Pirsel, Cancer Research Institute, Slovak Academy of Sciences, Bratislava (Slovakia). Penicillin streptomycin, RPMI 1640 GlutaMAX (where RPMI = Roswell Park Memorial Institute), and DMEM GlutaMAX media (where DMEM = Dulbecco's modified Eagle medium) were obtained from Life Technologies, and fetal bovine serum (FBS) was obtained from Merck. The cells were cultured in RPMI 1640 GlutaMAX (A2780, A2780cisR and Y79) and DMEM GlutaMAX (HEK-293) media containing 10% heat-inactivated FBS and 1% penicillin streptomycin at 37 °C and CO_2 (5%). The A2780cisR cell line was routinely treated with cisplatin (2 μM) in the media to maintain cisplatin resistance. The cytotoxicity was determined using the 3-(4,5-dimethyl 2-thiazolyl)-2,5-diphenyl-2H-tetrazolium bromide (MTT) assay.[35] Cells were seeded in flat-bottomed 96-well plates as a suspension in a prepared medium (100 μL aliquots and approximately 4300 cells/well) and preincubated for 24 h. Stock solutions of compounds were prepared in DMSO and were diluted in the medium. The solutions were sequentially diluted to give a final DMSO concentration of 0.5% and a final compound concentration range (0−200 μM). Cisplatin and RAPTA-C were tested as positive (0−100 μM) and negative (200 μM) controls respectively. The compounds were added to the preincubated 96-well plates in 100 μL aliquots, and the plates were incubated for a further 72 h. MTT (20 μL, 5 mg/mL in Dulbecco's phosphate buffered saline) was added to the cells, and the plates were incubated for a further 4 h. The culture medium was aspirated and the purple formazan crystals, formed by the mitochondrial dehydrogenase activity of vital cells, were dissolved in DMSO (100 μL/well). The absorbance of the resulting solutions, directly proportional to the

number of surviving cells, was quantified at 590 nm using a SpectroMax M5e multimode microplate reader (using SoftMax Pro software, version 6.2.2). The percentage of surviving cells was calculated from the absorbance of wells corresponding to the untreated control cells. The reported IC_{50} values are based on the means from two independent experiments, each comprising four tests per concentration level.

Cellular uptake. A2780 cells were seeded at a density of $2x10^6$ cells/Petri dish and incubated overnight. The cells were treated with the tested compounds at the concentrations and times given in the respective table. Following the treatment, the cells were harvested (trypsin), washed and pelleted. The pellets were digested with HCl using a microwave digestion system (CEM Mars). The Ru/Ir amount was determined with ICP-MS.

DNA metalation. After the treatment (see above), the cells were lyzed using DNAzol (DNAzol, MRC) reagent and following the manufacturer´s protocol. The DNA content was determined spectrophotometrically; the samples were lyzed in 30% hydrochloric acid (Suprapur, Merck Millipore) and the metal content was quantified by ICP-MS.

Enzyme inhibition assays. Preparation of cell lysates for analysis of enzyme activities. HeLa cells were seeded at a density of 3×10^5 cells/dish and incubated at 37 °C. The next day, the cells were treated with the investigated compounds or mixtures of their respective components at concentrations corresponding to the compounds´ IC_{50} values determined previously with MTT assay after 72 h. Following a further 18-h treatment, the cells were scraped, washed with PBS and counted. Identical cell counts were pelleted and lyzed in PBS-based lysis buffer (1% NP40, 1 mM PMSF, cocktail of protease inhibitors) on ice for 15 min. The supernatant was cleared and immediately subjected to enzyme activity analysis.

Analysis of glutathione S-transferase activity. The enzyme activity was evaluated with Glutathione S-Transferase Fluorescent Activity Kit (Invitrogen™) following the manufacturer´s protocol. Briefly, the cell lysates were plated in several dilutions in the Assay Buffer. Master mix containing Detection Reagent and Glutathione was added to the wells. The fluorescence was read in a kinetic mode at 460 nm with

excitation at 390 nm. After blank subtraction, the data were plotted as ΔRFU in the initial 5 min of the reaction. Data from 3-5 measurements were normalized to data of non-treated control cells.

Analysis of cyclooxygenase (COX) activity. The enzyme activity was evaluated with Cyclooxygenase Activity Assay Kit (Fluorometric) (Abcam) following the manufacturer´s protocol. Briefly, the cell lysates were plated in several dilutions in Assay Buffer. Then the Reaction Mix containing COX Probe and COX Cofactor was added to each well. The reaction was initiated with the addition of Arachidonic Acid/NaOH Solution. The fluorescence was read in a kinetic mode at 587 nm with excitation at 535 nm. After blank subtraction, the data were plotted as ΔRFU in the initial 5 min of the reaction. Data from 3-5 measurements were normalized to data of non-treated control cells.

Conflicts of interest

There are no conflicts to declare.

Acknowledgements

We gratefully thank the University of Pisa (Fondi di Ateneo 2020 and PRA_2020_39), the Czech Science Foundation (Grant 20-14082J) and the Swiss National Science Foundation for financial support.

Supporting Information Available

Characterization of compounds, including IR, NMR and MS spectra. X-ray diffraction. Solution stability studies (NMR data). CCDC reference number 2063385 ([**6**]BF_4) contains the supplementary crystallographic data for the X-ray study reported in this paper. These data can be obtained free of charge at https://www.ccdc.cam.ac.uk/structures/ (or from the Cambridge Crystallographic Data Centre, 12, Union Road, Cambridge CB2 1EZ, UK; e-mail: deposit@ccdc.cam.ac.uk).

References

1 (a) Štarha, P.; Trávníček, Z. Non-platinum complexes containing releasable biologically active ligands. *Coord. Chem. Rev*. **2019**, *395*, 130-145. (b) Kenny, R. G.; Marmion, C. J. Toward Multi-Targeted Platinum and Ruthenium Drugs-A New Paradigm in Cancer Drug Treatment Regimens? *Chem. Rev.* **2019**, *119*, 1058–1137. (c) Khoury, A.; Deo, K. M.; Aldrich-Wright, J. R. Recent advances in platinum-based chemotherapeutics that exhibit inhibitory and targeted mechanisms of action. *J. Inorg. Biochem*. **2020**, *207*, 111070. (d) Boros, E.; Dyson, P. J.; Gasser, G. Classification of Metal-based Drugs According to Their Mechanisms of Action. *Chem.* **2020**, *6*, 41-60.

2 Selected references: (a) Ang, W. H.; Khalaila, I.; Allardyce, C. S.; Juillerat-Jeanneret, L.; Dyson, P. J. Rational design of platinum(IV) compounds to overcome glutathione-S-transferase mediated drug resistance. *J. Am. Chem. Soc.* **2005**, *127*, 1382–1383. (b) Cheng, Q.; Shi, H.; Wang, H.; Wang, J.; Liu, Y. Asplatin enhances drug efficacy by altering the cellular response. Metallomics **2016** *8*, 672-678. (c) Nazarov, A. A.; Meier, S. M.; Zava, O.; Nosova, Y. N.; Milaeva, E. R.; Hartinger, C. G.; Dyson, P. J. Protein ruthenation and DNA alkylation: chlorambucil-functionalized RAPTA complexes and their anticancer activity. *Dalton Trans*. **2015**, *44*, 3614-3623. (d) Yang, J.; Sun, X.; Mao, W.; Sui, M.; Tang, J.; Shen, Y. Conjugate of Pt(IV)–Histone Deacetylase Inhibitor as a Prodrug for Cancer Chemotherapy, Mol. Pharm. **2012**, *10*, 2793–2800; (e) Dhar, S.; Lippard, S. J. Mitaplatin, a potent fusion of cisplatin and the orphan drug dichloroacetate. *Proc. Natl. Acad. Sci. USA* **2009**, *106*, 22199-22204. (f) Petruzzella, E.; Phillip Braude, J.; Aldrich-Wright, J. R.; Gandin, V.; D. Gibson, A Quadruple-Action Platinum(IV) Prodrug with Anticancer Activity Against KRAS Mutated Cancer Cell Lines. *Angew. Chem.* **2017**, *56*, 11539-11544.

3 Gibson, D.; Platinum(IV) anticancer agents; are we en route to the holy grail or to a dead end? *J. Inorg. Biochem.* **2021**, *217*, 111353.

4 (a) Hu, W.; Fang, L.; Hua, W.; Gou, S. Biotin-Pt (IV)-indomethacin hybrid: A targeting anticancer prodrug providing enhanced cancer cellular uptake and reversing cisplatin resistance. *J. Inorg. Biochem*. **2017**, 175, 47–57. (b) Petruzzella, E.; Sirota, R.; Solazzo, I.; Gandin, V.; Gibson, D. Triple action Pt(IV) derivatives of cisplatin: a new class of potent anticancer agents that overcome resistance. *Chem. Sci*. **2018**, *9*, 4299. (c) Babak, M. V.; Zhi, Y.; Czarny, B.; Boon Toh, T.; Hooi, L.; Kai-Hua Chow E.; Ang, W. H.; Gibson, D.; Pastorin, G. Dual-Targeting Dual-Action Platinum(IV) Platform for Enhanced Anticancer Activity and Reduced Nephrotoxicity. *Angew. Chem. Int. Ed*. **2019**, *58*, 8109–8114. (d) Karmakar, S.; Poetsch, C.; Kowol, R.; Heffeter, P.; Gibson, D. Synthesis and Cytotoxicity of Water-Soluble Dual- and Triple-Action Satraplatin Derivatives: Replacement of Equatorial Chlorides of Satraplatin by Acetates. *Inorg. Chem*. **2019**, *58*, 16676−16688. (e) Shi, H.;

Imberti, C.; Huang, H.; Hands-Portman, I.; Sadler, P. J. Biotinylated photoactive Pt(IV) anticancer complexes. *Chem. Commun*. **2020**, *56*, 2320-2323; (f) Babu, T.; Sarkar, A.; Karmakar, S.; Schmidt, C.; Gibson, D. Multiaction Pt(IV) Carbamate Complexes Can Codeliver Pt(II) Drugs and Amine Containing Bioactive Molecules. *Inorg. Chem*. **2020**, *59*, 5182−5193. (g) Muhammad, N.; Tan, C.-P.; Nawaz, U.; Wang, J.; Wang, F.-X.; Nasreen, S.; Ji, L.-N.; Mao, Z.-W. Multiaction Platinum(IV) Prodrug Containing Thymidylate Synthase Inhibitor and Metabolic Modifier against Triple-Negative Breast Cancer. *Inorg. Chem.* **2020**, *59*, 12632−12642. (h) Karmakar, S.; Kostrhunova, H.; Ctvrtlikova, T.; Novohradsky, V.; Gibson, D.; Brabec, V. Platinum(IV)-Estramustine Multiaction Prodrugs Are Effective Antiproliferative Agents against Prostate Cancer Cells. *J. Med. Chem*. **2020**, *63*, 13861−13877.

5 Biancalana, L.; Batchelor, L. K.; Pereira, S. A. P.; Tseng, P.-J.; Zacchini, S.; Pampaloni, G.; Saraiva, L. M. F. S.; Dyson, P. J.; Marchetti F. Bis-conjugation of Bioactive Molecules to Cisplatin-like Complexes through (2,2′-Bipyridine)-4,4′-Dicarboxylic Acid with Optimal Cytotoxicity Profile Provided by the Combination Ethacrynic Acid/Flurbiprofen. *Chem. Eur. J.* **2020**, *26*, 17525-17535.

6 (a) Nazarov, A. A.; Hartinger, C. G.; Dyson, P. J. Opening the lid on piano-stool complexes: an account of ruthenium (II)–arene complexes with medicinal applications. *J. Organomet. Chem*. **2014**, *751*, 251-260. (b) Murray, B. S.; Babak, M. V.; Hartinger, C. G.; Dyson, P. J. The development of RAPTA compounds for the treatment of tumors. *Coord. Chem. Rev*. **2016**, *306*, 86–114. (c) Anthony, E. J.; Bolitho, E. M.; Bridgewater, H. E.; Carter, O. W. L.; Donnelly, J. M.; Imberti, C.; Lant, E. C.; Lermyte, F.; Needham, R. J.; Palau, M.; Sadler, P. J.; Shi, H.; Wang, F.-X.; Zhang, W.-Y.; Zhang, Z. Metallodrugs are unique: opportunities and challenges of discovery and development. *Chem. Sci*. **2020**, *11*, 12888–12917. (d) Meier-Menches, S. M.; Gerner, C.; Berger, W.; Hartinger, C. G.; Keppler, B. K. Structure–activity relationships for ruthenium and osmium anticancer agents – towards clinical development. *Chem. Soc. Rev*. **2018**, *47*, 909-928. (e) J. J. Soldevila-Barreda, N. Metzler-Nolte, Intracellular Catalysis with Selected Metal Complexes and Metallic Nanoparticles: Advances toward the Development of Catalytic Metallodrugs. *Chem. Rev*. **2019**, *119*, 829–869.

7 (a) Movassaghi, S.; Leung, E.; Hanif, M.; Lee, B. Y. T.; Holtkamp, H. U.; Tu, J. K. Y.; Söhnel, T.; Jamieson, S. M. F.; Hartinger, C. G. A Bioactive L-Phenylalanine-Derived Arene in Multitargeted Organoruthenium Compounds: Impact on the Antiproliferative Activity and Mode of Action. *Inorg. Chem*. **2018**, *57*, 8521–8529; (b) Biancalana, L.; Gruchała, M.; Batchelor, L. K.; Błauż, A.; Monti, A.; Pampaloni, G.; Rychlik, B.; Dyson, P. J.; Marchetti, F. Conjugating Biotin to Ruthenium(II) Arene Units via Phosphine Ligand Functionalization. *Eur. J. Inorg. Chem*. **2020**, *11-12*, 1061-1072.

8 (a) Hayes, J. D.; Flanagan, J. U.; Jowsey, I. R. Glutathione transferases. *Ann. Rev. Pharmacol. Toxicol*. **2005**, *45*, 51–88. (b) Townsend D. M.; Findlay V. L.; Tew K. D., Glutathione S-Transferases as Regulators of Kinase Pathways and Anticancer Drug Targets, Methods in Enzymol. 2005, 401, 287-307.

9 (a) Ang, W. H.; Parker, L. J.; De Luca, A.; Juillerat-Jeanneret, L.; Morton, C. J.; Lo Bello, M.; Parker, M. W.; Dyson, P. J. Rational design of an organometallic glutathione transferase inhibitor. *Angew. Chem. Int. Ed*. **2009**, *48*, 3854-3857. (b) Agonigi, G.; Riedel, T.; Zacchini, S.; Paunescu, E.; Pampaloni, G.; Bartalucci, N.; Dyson, P. J.; Marchetti, F. Synthesis and Antiproliferative Activity of New Ruthenium Complexes with Ethacrynic Acid-Modified Pyridine- and Triphenylphosphine-Ligands. *Inorg. Chem*. **2015**, *54*, 6504–6512. (c) Păunescu, E.; Soudani, M.; Martin, P.; Scopelliti, R.; Lo Bello, M.; Dyson, P. J. Organometallic Glutathione S-Transferase Inhibitors. *Organometallics* **2017**, *36*, 3313-3321.

10 (a) Knights, K. M.; Mangoni, A. A.; Miners, J. O. Defining the COX inhibitor selectivity of NSAIDs: implications for understanding toxicity. *Expert Rev. Clin. Pharmacol*. **2010**, *3*, 769-776. (b) Regulski, M.; Regulska, K.; Prukała, W.; Piotrowska, H.; Stanisz, B.; Murias, M.; COX-2 inhibitors: a novel strategy in the management of breast cancer. *Drug Disc. Tod*. **2016**, *21*, 598-615. (c) Tan, J.; Li, C.; Wang, Q.; Li, S.; Chen, S.; Zhang, J.; Wang, P. C.; Ren L.; Liang, X.-J. A Carrier-Free Nanostructure Based on Platinum(IV) Prodrug Enhances Cellular Uptake and Cytotoxicity. *Mol. Pharmaceutics* **2018**, *15*, 1724−1728.

11 (a) Raja, M. U.; Tauchman, J.; Therrien, B.; Süss-Fink, G.; Riedel, T.; Dyson P. J. Arene ruthenium and pentamethylcyclopentadienyl rhodium and iridium complexes containing N,O-chelating ligands derived from piroxicam: Synthesis, molecular structure and cytotoxicity. *Inorg. Chim. Acta* **2014**, *409*, 479–483. (b) Paunescu, E.; McArthur, S.; Soudani, M.; Scopelliti, R.; Dyson P. J. Nonsteroidal Anti-inflammatory Organometallic Anticancer Compounds. *Inorg. Chem*. **2016**, *55*, 1788−1808. (c) Biancalana, L.; Batchelor, L. K.; De Palo, A.; Zacchini, S.; Pampaloni, G. Dyson, P. J.; Marchetti F. A general strategy to add diversity to ruthenium arene complexes with bioactive organic compounds via a coordinated (4-hydroxyphenyl)diphenylphosphine ligand, *Dalton Trans*. **2017**, *46*, 12001-12004. (d) Ashraf, A.; Aman, F.; Movassaghi, S.; Zafar, A.; Kubanik, M.; Siddiqui, W. A.; Reynisson, J. H.; Söhnel, T.; Jamieson, S. M.; Hanif, M. Structural Modifications of the Antiinflammatory Oxicam Scaffold and Preparation of Anticancer Organometallic Compounds. *Organometallics* **2019**, *38*, 361–374.

12 (a) Maiti, S.; Paira, P. Biotin conjugated organic molecules and proteins for cancer therapy: A review. *Eur. J. Med. Chem*. **2018**, *145*, 206-223. (b) Bertrand, B.; O'Connell, M. A.; Waller, Z. A.

E.; Bochmann, M. A Gold(III) Pincer Ligand Scaffold for the Synthesis of Binuclear and Bioconjugated Complexes: Synthesis and Anticancer Potential. *Chem. Eur. J*. **2018**, *24*, 3613–3622. (c) Côrte-Real, L.; Karas; B. Bras, A. R.; Pilon, A.; Avecilla, F.; Marques, F.; Preto, A.; Buckley, B. T.; Cooper, K. R.; Doherty, C.; Garcia M. H.; Valente, A. Ruthenium–Cyclopentadienyl Bipyridine–Biotin Based Compounds: Synthesis and Biological Effect. *Inorg. Chem*. **2019**, *58*, 9135−9149; (d) Plazuk, D.; Zakrzewski, J.; Salmain, M.; Błauz, A.; Rychlik, B.; Strzelczyk, P.; Bujacz, A.; Bujacz, G. Ferrocene–Biotin Conjugates Targeting Cancer Cells: Synthesis, Interaction with Avidin, Cytotoxic Properties and the Crystal Structure of the Complex of Avidin with a Biotin–Linker–Ferrocene Conjugate. *Organometallics* **2013**, *32*, 5774−5783.

13 (a) Wu, S.; Zhou, Y.; Rebelein, J. G.; Kuhn, M.; Mallin, H.; Zhao, J.; Igareta, N. V.; Ward T. R. Breaking Symmetry: Engineering Single-Chain Dimeric Streptavidin as Host for Artificial Metalloenzymes. *J. Am. Chem. Soc*. **2019**, *141*, 15869–15878. (b) Okamoto, Y.; Köhler, V.; Paul, C. E.; Hollmann, F.; Ward T. R. Efficient In Situ Regeneration of NADH Mimics by an Artificial Metalloenzyme. *ACS Catal*. **2016**, *6*, 3553–3557. (c) Muñoz Robles, V.; Dürrenberger, M.; Heinisch, T.; Lledós, A.; Schirmer, T.; Ward, T. R.; Maréchal J.-D. Structural, Kinetic, and Docking Studies of Artificial Imine Reductases Based on Biotin–Streptavidin Technology: An Induced Lock-and-Key Hypothesis. *J. Am. Chem. Soc*. **2014**, *136*, 15676–15683.

14 (a) Lewandowski, E. M.; Skiba, J.; Torelli, N. J.; Rajnisz, A.; Solecka, J.; Kowalski, K.; Chen, Y. Antibacterial properties and atomic resolution X-ray complex crystal structure of a ruthenocene conjugated β-lactam antibiotic. *Chem. Commun*. **2015**, *51*, 6186-6189. (b) Skiba, J.; Rajnisz, A.; Navakoski de Oliveira, K.; Ott, I.; Solecka, J.; Kowalski, K. Ferrocenyl bioconjugates of ampicillin and 6-aminopenicillinic acid--synthesis, electrochemistry and biological activity. *Eur. J. Med. Chem*. **2012**, *57*, 234-239; (c) Ketikidis, J.; Banti, C. N.; Kourkoumelis, N.; Tsiafoulis, C. G.; Papachristodoulou, C.; Kalampounias, A. G.; Hadjikakou, S. K. Conjugation of Penicillin-G with Silver(I) Ions Expands Its Antimicrobial Activity against Gram Negative Bacteria. *Antibiotics* **2020**, *9*, 25.

15 (a) Wheate, N. J.; Walker, S.; Craig, G. E.; Oun, R. The status of platinum anticancer drugs in the clinic and in clinical trials. *Dalton Trans.* **2010**, *39*, 8113–8127. (b) Yu, C.; Wang, Z.; Sun, Z.; Zhang, L.; Zhang, W.; Xu, Y.; Zhang, J.-J. Platinum-Based Combination Therapy: Molecular Rationale, Current Clinical Uses, and Future Perspectives. *J. Med. Chem*. **2020**, *63*, 13397-13412.

16 (a) Zhang, D.; Dufek E. J.; Clennan, E. L. Syntheses, Characterizations, and Properties of Electronically Perturbed 1,1‘-Dimethyl-2,2‘-bipyridinium Tetrafluoroborates. *J. Org. Chem*. **2006**, *71*, 315–319. (b) Miyoshi, D.; Karimata, H.; Wang, Z.-M.; Koumoto, K.; Sugimoto, N. Artificial G-

Wire Switch with 2,2‘-Bipyridine Units Responsive to Divalent Metal Ions. *J. Am. Chem. Soc*. **2007**, *129*, 5919–5925.

17 To the best of our knowledge, only a few transition metal benzylpenicillin complexes have been reported in the literature. (a) Grochowski, T.; Samochoka, K. Structural Characterization of the Platinum(II)-Penicillin Complexes. *Polyhedron* **1991**, *10*, 1473-1477; (b) Spectroscopic and Thermal Investigations of Transition and Non-Transition Metal Complexes of Penicillin G as Potential Biological Active Species. Refata, M. S.; Al-Saif, F. A. *Russ. J. Gen. Chem*. **2014**, *84*, 143–156 (characterization limited to IR spectroscopy and magnetic analysis).

18 The cation [**6**]$^{+}$ was previously reported as chloride salt. Brewster, T. P.; Miller, A. J. M.; Heinekey, D. M.; Goldberg, K. I. Hydrogenation of Carboxylic Acids Catalyzed by Half-Sandwich Complexes of Iridium and Rhodium. *J. Am. Chem. Soc*. **2013**, *135*, 16022−16025.

19 The maximum amount of water in these experiments - thus the DMSO/water ratio - is limited by the solubility of the compounds and the millimolar concentration required for a good quality ^{1}H NMR spectrum.

20 (a) Bugarcic, T.; Habtemariam, A.; Stepankova, J.; Heringova, P.; Kasparkova, J.; Deeth, R. J.; Johnstone, R. D. L.; Prescimone, A.; Parkin, A.; Parsons, S.; Brabec, V.; Sadler P. J. The Contrasting Chemistry and Cancer Cell Cytotoxicity of Bipyridine and Bipyridinediol Ruthenium(II) Arene Complexes. *Inorg. Chem*. **2008**, *47*, 11470-11486. (b) Liu, Z.; Habtemariam, A.; Pizarro, A. M.; Fletcher, S. A.; Kisova, A.; Vrana, O.; Salassa, L.; Bruijnincx, P. C. A.; Clarkson, G. J.; Brabec, V.; Sadler, P. J.; Organometallic Half-Sandwich Iridium Anticancer Complexes, *J. Med. Chem*. **2011**, *54*, 3011–3026.

21 For ethacrynic acid: (a) Wang, R.; Li, C.; Song, D.; Zhao, G.; Zhao, L.; Jing Y. Ethacrynic Acid Butyl-Ester Induces Apoptosis in Leukemia Cells through a Hydrogen Peroxide–Mediated Pathway Independent of Glutathione S-Transferase P1-1 Inhibition, *Cancer Res* **2007**, *67*, 7856-7564; (b) Agonigi, G.; Riedel, T.; Pilar Gay, M.; Biancalana, L.; Oñate, E.; Dyson, P. J.; Pampaloni, G.; Paunescu, E.; Esteruelas, M. A.; Marchetti F. Arene Osmium Complexes with Ethacrynic Acid-Modified Ligands: Synthesis, Characterization, and Evaluation of Intracellular Glutathione S-Transferase Inhibition and Antiproliferative Activity, *Organometallics* **2016**, *35*, 1046–1056; (c) Mignani S.; El Brahmi N.; El Kazzouli S.; Eloy L.; Courilleau D.; Caron J.; Bousmina M. M.; Caminade A.-M.; Cresteil T.; Majoral J.-P. A novel class of ethacrynic acid derivatives as promising drug-like potent generation of anticancer agents with established mechanism of action. *Eur. J. Med. Chem*. **2016**, *122*, 656-673.

22 (a) Schmitt, F.; Kasparkova, J.; Brabec, V.; Begemann, G.; Schobert, R.; Biersack, B. New (arene)ruthenium(II) complexes of 4-aryl-4H-naphthopyrans with anticancer and anti-vascular activities. *J. Inorg. Biochem*. **2018**, *184*, 69. (b) Novohradsky, V.; Zerzankova, L.; Stepankova, J.; Kisova, A.; Kostrhunova, H.; Liu, Z.; Sadler, P. J.; Kasparkova, J.; Brabec, V. A dual-targeting, apoptosis-inducing organometallic half-sandwich iridium anticancer complex. *Metallomics* **2014**, *6*, 1491-501.

23 Ethacrynic acid (CAS 58-54-8): 2,3-dichloro-4-(2-methylene-1-oxobutyl)phenoxyacetic acid. Flurbiprofen (CAS 5104-49-4): (±)-2-fluoro-α-methyl-(1,1'-biphenyl)-4-acetic acid (racemic mixture). Biotin (CAS 58-85-5): 5-[(3aS,4S,6aR)-2-oxohexahydro-1H-thieno[3,4-d]imidazol-4-yl]pentanoic acid. Potassium benzylpenicillin (CAS 113-98-4): potassium (2S,5R,6R)-3,3-dimethyl-7-oxo-6-[(phenylacetyl)amino]-4-Thia-1-azabicyclo[3.2.0]heptane-2-carboxylate.

24 (a) Bennett, M. A.; Smith, A. K.; Arene ruthenium(II) complexes formed by dehydrogenation of cyclohexadienes with ruthenium(III) trichloride. *J. Chem. Soc., Dalton Trans*. **1974**, 233-241. (b) Optimized procedure: Biancalana, L.; Zacchini, S.; Ferri, N.; Lupo, M. G.; Pampaloni, G.; Marchetti, F. Tuning the cytotoxicity of ruthenium(II) para-cymene complexes by mono-substitution at a triphenylphosphine/phenoxydiphenylphosphine ligand. *Dalton Trans*. **2017**, *46*, 16589-16604.

25 White, C.; Yates, A.; Maitlis, P. M. (η^5-pentamethylcyclopentadienyl)rhodium and -iridium compounds. *Inorg. Synth.* **1992**, *29*, 228-234.

26 Fulmer, G. R.; Miller, A. J. M.; Sherden, N. H.; Gottlieb, H. E.; Nudelman, A.; Stoltz, B. M.; Bercaw, J. E.; Goldberg, K. I. NMR Chemical Shifts of Trace Impurities: Common Laboratory Solvents, Organics, and Gases in Deuterated Solvents Relevant to the Organometallic Chemist. *Organometallics* **2010**, *29*, 2176–2179.

27 Harris, R. K.; Becker, E. D.; Cabral De Menezes, S. M.; Goodfellow, R.; Granger, P. NMR nomenclature. Nuclear spin properties and conventions for chemical shifts (IUPAC Recommendations 2001). *Pure Appl. Chem.* **2001**, *73*, 1795–1818.

28 Willker, W.; Leibfritz, D.; Kerssebaum, R.; Bermel, W. Gradient selection in inverse heteronuclear correlation spectroscopy. *Magn. Reson. Chem*. **1993**, *31*, 287-292.

29 Menges, F. "Spectragryph - optical spectroscopy software", Version 1.2.14d, @ 2016-2020, http://www.effemm2.de/spectragryph.

30 A solution of $[IrCl_2(\eta^5\text{-}C_5Me_5)]_2$ (29 mg, 0.036 mmol) in MeOH (5 mL) was treated with $AgNO_3$ (12 mg, 0.073 mmol) and stirred at room temperature in the dark. After 1 h, the mixture was filtered over a celite pad and $\mathbf{L}^{\boldsymbol{EB}}$ (66 mg, 0.078 mmol) was added to the yellow filtrate solution. The suspension was stirred at reflux for 15 h, affording an orange solution. NMR analysis (^{1}H, $CDCl_3$)

revealed a mixture of [**6**]$^+$, ***B*-$CO_2(CH_2)_2OH$**, ***E*-$CO_2(CH_2)_2OH$** and ***E*-CO_2H** (1:1:0.8:0.2 molar ratio).

31 Sheldrick, G. M. SADABS-2008/1 - Bruker AXS Area Detector Scaling and Absorption Correction, Bruker AXS: Madison, Wisconsin, USA, 2008

32 Sheldrick, G. M. Crystal Structure Refinement with SHELXL. *Acta Crystallogr. C* **2015**, *71*, 3-8.

33 Rundlöf, T.; Mathiasson, M.; Bekiroglu, S.; Hakkarainen, B.; Bowden, T.; Arvidsson, T. Survey and qualification of internal standards for quantification by 1H NMR spectroscopy. *J. Pharm. Biomed. Anal.* **2010**, *52*, 645–651.

34 ^{14}N and ^{35}Cl NMR reference data. All data refer to the pure compounds dissolved the selected solvent. NaCl. ^{35}Cl NMR ($8.8\cdot10^{-2}$ M, DMSO/H_2O 5:1, few scans): δ/ppm = 44.6 ($\Delta\nu_{1/2}$ = 545 Hz). KCl. ^{35}Cl NMR ($1.9\cdot10^{-2}$ M, DMSO/H_2O 5:1, few scans): δ/ppm = 41.2 ($\Delta\nu_{1/2}$ = 447 Hz). NaNO3. ^{14}N NMR (DMSO/H_2O 5:1): δ/ppm = −5.1 ($\Delta\nu_{1/2}$ = 23 Hz).

35 Mosmann, T. Rapid colorimetric assay for cellular growth and survival: application to proliferation and cytotoxicity assays. *J. Immunol. Methods* **1983**, *65*, 55–63.

Table of Contents graphic and synopsis

Synergic effects on cytotoxicity, metal uptake and enzyme inhibition on cancer cells are provided by the association of two different bioactive organic molecules (ethacrynic acid and flurbiprofen) to Ru(II)-*p*-cymene and Ir(III) pentamethylcyclopentadienyl complexes, via a robust 2,2'-bipyridine ligand.